

Numerical simulation on the ice load acting on ARAON using damage-based erosion model

Sangkyu Jeon¹, Yooil Kim¹

¹Department of Naval Architecture and Ocean Engineering, INHA University, 100, Inha-Ro, Nam-Gu, Incheon, South Korea

ABSTRACT

This paper presents an advanced numerical analysis technique to simulate the level ice-ship interaction phenomenon using finite element method. To simulate ice breaking phenomenon with reality, the traditional Drucker–Prager plasticity model was combined with damage mechanics and linked with the element erosion technique to realize crack formation and propagation in level ice colliding with a moving structure. In order to capture dynamic motions of submerged broken ice flakes, both dynamic drag forces and static buoyancy forces were taken into account. Using the model described above, the ice resistance acting on a rigid ship running through level ice with different forward speeds was numerically calculated and compared with model basin test results obtained in ice tank. Also, efforts were made to decompose total ice resistance into breaking and submergence ones by running additional simulation where ice flakes were removed right after breaking.

KEY WORDS: Finite element method; Level ice; Damage mechanics; Drucker-Prager; Element erosion;

INTRODUCTION

Estimation method of ice load is classified as experimental method and numerical simulation. The experimental method includes a full-scale measurement from a database of structures operating in the arctic ocean and a model-scale measurement using model ship and ice tank. Although the full-scale measurement data are intuitive, it is difficult to figure out the effect of sea ice parameters such as ice thickness, bending strength and friction coefficient on ice load only by load history. Therefore, the model-scale measurement was an important alternative to understanding ice load because it can be estimated by controlling these parameters. However, the model-scale measurement is limited depending on the capacity of the ice tank and it is not easy to optimally design structure in terms of cost and time. As a result, a numerical method was required and many research efforts have been made recently relying on numerical simulation in line with recent improvements of computer performance.

Lubbad and Løset (2011) calculated the ice load in a semi-analytic approach in time domain according to the fracture mode of ice using some assumptions. Lu (2014) conducted finite element analysis using cohesive elements and performed calculation of ice load and decomposition ice load component on downward conical structures through experiment and

numerical simulation. Kim and Kim (2019) used periodic media analysis technique to calculate long term fatigue of finite element model passing through the broken ice field according to different concentration.

In this paper, the test performed in Korea Research Institute of Ships and Ocean Engineering (KRISO) by Jeong (2016) was modeled according to modeling technique of structure level ice interaction proposed by Jeon and Kim (2021). And components of ice load were divided to breaking and submersion load component removing submerged ice flakes that reached a certain criteria. The result of present study was compared with that of test.

THEORETICAL BACKGROUND

Linear DP plasticity model

As yield criteria of ice, linear Drucker-Prager plasticity, where the relationship between hydrostatic stress and deviatoric stress is linear in π -plane, is used. The Drucker-Prager yield criterion adds hydrostatic stress effect to the previously known von Mises yield criterion, and the yield surface is conical from a three-dimensional principal stress space. Eq(1) is the yield function of the Drucker-Prager, which means that the material reaches the yield criteria when this function reaches zero.

$$F = q + p \tan(\beta) + d = 0 \quad (1)$$

where q is von Mises stress, p is hydrostatic stress and β, d is material properties obtained by triaxial compression test.

$$p = -\frac{1}{3} \text{trace}(\sigma) \quad (2)$$

$$S = \sigma + pI \quad (3)$$

$$q = \sqrt{\frac{3}{2} (S:S)} = \sqrt{\frac{3}{2} J_2} \quad (4)$$

where σ is the stress tensor, S is the deviatoric stress and J_2 is second stress invariant.

Damage model

Ice is a material dependent on the strain rate, which known as brittle behavior at high strain rates. Ship-ice interaction occurs relatively at high interaction velocity. therefore, it is common to assume that the behavior of the ice is brittle, which means that the complex behavior of the plastic region is ignored. To define this behavior, we revised general damage model of Figure 1-(a) to a modified model of Figure 1-(b)

$$\omega_D = \int \frac{d\bar{\epsilon}^{pl}}{\bar{\epsilon}_o^{pl} (\eta, \dot{\bar{\epsilon}}^{pl})} \quad (5)$$

State variable w_D defines point at which the damage initiation occurs as a fracture strain. Deformation energy induced to the process of evolution from the generation of equivalent plastic strain to fracture is defined fracture energy G_f as Eq(6). L is the length of the element where the fracture occurs.

$$G_f = \int_{\bar{\varepsilon}_0^{pl}}^{\bar{\varepsilon}_f^{pl}} L \sigma_y d\bar{\varepsilon}^{pl} = \int_0^{\bar{\varepsilon}_f^{pl}} \sigma_y d\bar{u}^{pl} \quad (6)$$

Assuming that the relationship between the equivalent plastic displacement and Damage variable is linear and performing the integral of Eq(6), the damage variable in Eq(7) is finally obtained.

$$D = \frac{\bar{u}^{pl} \sigma_{y0}}{2G_f} \quad (7)$$

When the damage variable D reaches 1, elements will no longer have load carrying capacity and these will be removed and excluded from the calculation.

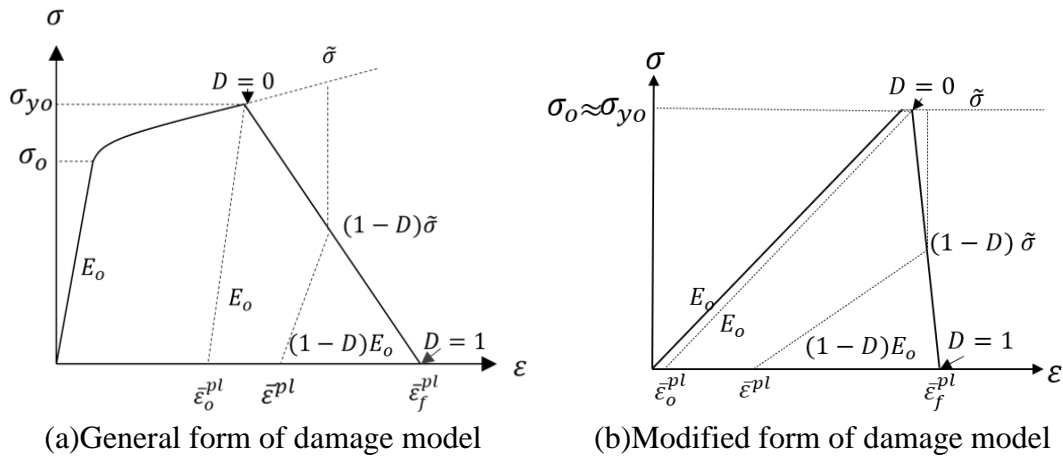


Figure 1. Damage model

Buoyancy and drag model

Buoyancy

The method for applying buoyancy to finite element models is as follows. A point where y is 0 is defined as a free surface, and surface force is defined as a hydrostatic pressure only when y is less than 0 as in Eq (8). By defining the surface area for both the external and internal surfaces of the element, buoyancy can be embodied in all cases included before and after the erosion of the element. For example, before the element disappears, the pressure applied on the inner face is the same magnitude and the direction is opposite, so the inner face cannot engage in buoyancy and only the outer face is applied to pressure. In addition, since surface force is also defined to the inner surface, buoyancy can be realized when applied to the pressure defined before for the newly exposed inner surface due to the erosion of elements.

$$p(x, y, z) = \begin{cases} p_w g h & (y < 0) \\ 0 & (y \geq 0) \end{cases} \quad (8)$$

where p_w is density of water, g is gravity and h is height of center of element surface

Drag model

Present study focused on approximately applying Rayleigh damping to the drag force acting on ice flakes. Eq **Ошибка! Источник ссылки не найден.** is the governing equation of finite element considered as Rayleigh damping, which is proportional to mass.

$$[M]\{\ddot{x}\} + \alpha[M]\{\dot{x}\} + [K]\{x\} = \{f\} \quad (9)$$

where $[M]$ is mass matrix, $[K]$ is stiffness matrix, $\{f\}$ is nodal external force vector, $\{x\}$ is displacement vector and α is damping factor. The factor is determined empirically because the drag acting on ice flakes are idealized by Rayleigh damping

Ice load contributions

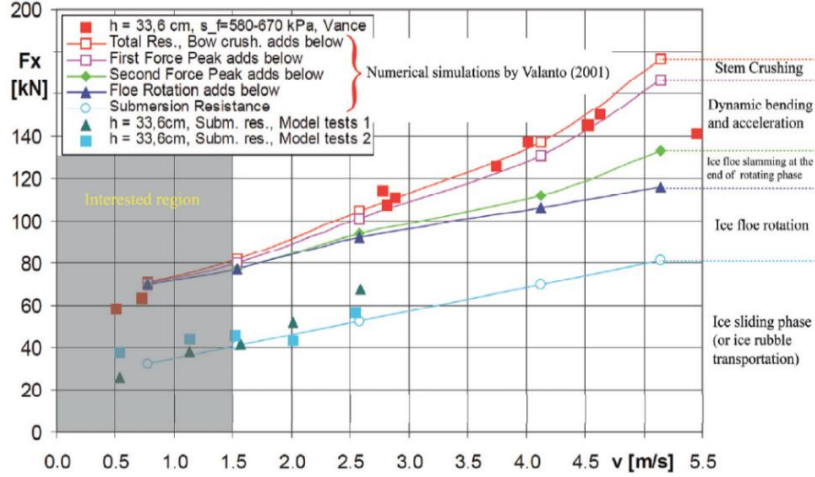


Figure 2. Comparative contributions of different load components vs interaction speed

Efforts have been made in the past to decompose the total ice resistance, induced by level ice, using either numerical and experimental method. Figure 2 shows the resistance components obtained from experiment of Lu (2014) together with the resistance component obtained from numerical simulation of Valanto (2001). The ice resistance component can be divided into five components, such as Eq(10).

$$R_{level} = R_c + R_b + R_s + R_r + R_{rt} \quad (10)$$

where R_c is resistance due to stem crushing, R_b is resistance due to dynamic bending and acceleration, R_s is resistance due to slamming at the end of rotating phase, R_r is resistance due to rotating motion of ice floe, R_{rt} is resistance due to rubble transportation. The overall trend of numerical simulation results shows that the contribution for the R_r and R_{rt} is significantly large in low speeds. And as the speed is higher, the rate of the increase in remaining components such as R_c , R_b is higher than R_{rt} . Eq(10) can be rewritten as Eq(13) by grouping the resistance into breaking and submersion one.

$$R_{breaking} = R_c + R_b \quad (11)$$

$$R_{submersion} = R_s + R_r + R_{rt} \quad (12)$$

$$R_{level} = R_{breaking} + R_{submersion} \quad (13)$$

LEVEL ICE-ARAON MODEL SHIP INTERACTION SIMULATION

FE model

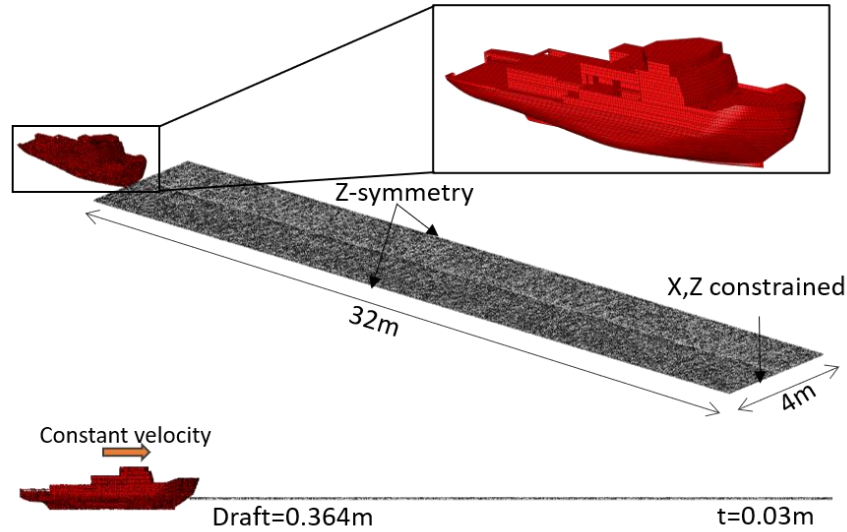


Figure 3. Assembly view of finite element model

The Figure 3 represents the finite element model applied to present study. The x-axis is the direction in which the hull moves forward, the y-axis is in the direction of gravity, and the z-axis is in the direction of the side of the hull. Symmetry conditions are assigned to both sides of the level ice as constraints. The displacement of end of level ice except for the y-direction was constrained so that the level ice did not move in the x-axis direction when colliding with the hull. The parameters of the Drucker-Prager yield surface were used with values of Zhang (2017), and the fracture energy was quoted from Lu (2014) with model scale ration of 18.667. In order to compare the load contribution with respect to three constant speed cases, two models were used for analysis: original model and rubble erosion model

Table 1. Material properties of level ice

Material property	Value	Unit
Young`s modulus	70	Mpa
Poisson`s ratio	0.3	-
Density	870	kg/m ³
Flexural strength	30	kPa
compressive strength	50	kPa
Friction angle	36	°
Dilation angle	12	-
Flow stress ratio	1	°
Fracture strain	1e-15	-
Fracture energy	0.043	N/m ²

Friction coefficient	0.05	-
----------------------	------	---

Result of original and rubble removal model

Fracture pattern of level ice

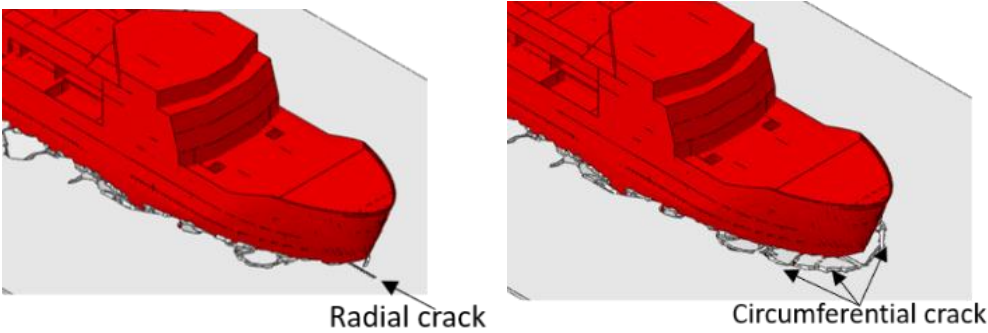


Figure 4. Fracture pattern of level ice

When a vertical load is applied to the contact point of the level ice by icebreaker, a radial crack occurs first. And a circumferential crack is formed at a place where bending strength is reached. Although irregularities in the free edge of level ice caused some complicated fracture patterns, radial and circumferential crack can be observed as Figure 4

Ice flakes analysis

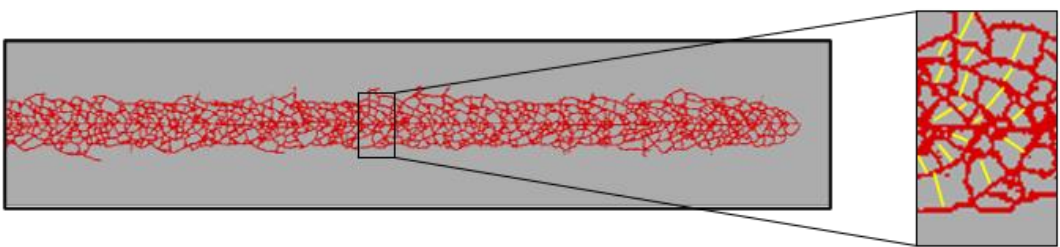


Figure 5. Procedure of calculation about length of cusp

To determine the size of the ice flakes, the length of cusp was calculated as shown in the yellow line of Figure 5. The cusp size distribution of Figure 6 shows the decrease of variance as the speed increases. And the Figure 7 shows that the mean flake sizes obtained from the simulation are a little larger than the experiment, but the magnitude itself decreases as the speed increases.

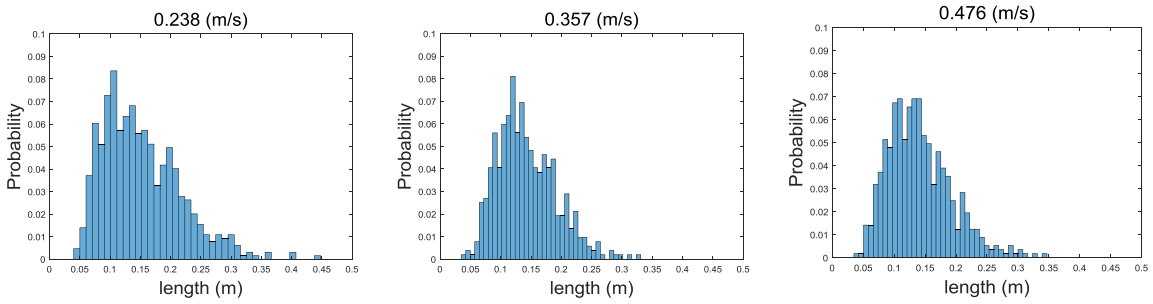


Figure 6. Probability distribution of cusp size

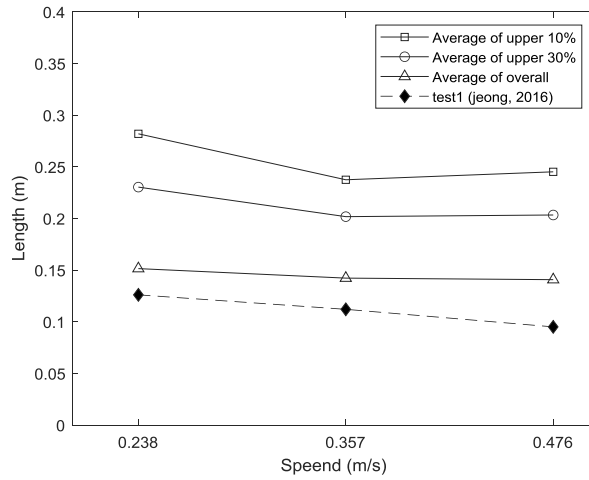


Figure 7. Comparison of cusp size with experimental data

Comparison of local ice load

Local ice load of the original model and the rubble removal model was compared to see influence on ice load. The load history of Figure 8 is for the panel highlighted in yellow circle on bow. Figure 8-(a) shows that the peak load has different fluctuations pattern depending on the collision phase, i.e. ice breaking phase and the rubble contact phase, in original model. The peak load is relatively steady in contacting rubble phase compared to the peak load in breaking phase. On the other hand, Figure 8-(b) shows that there is a free-run phase, corresponding to rubble contact phase in original model, where local load converges to zero because the ice flakes are removed.

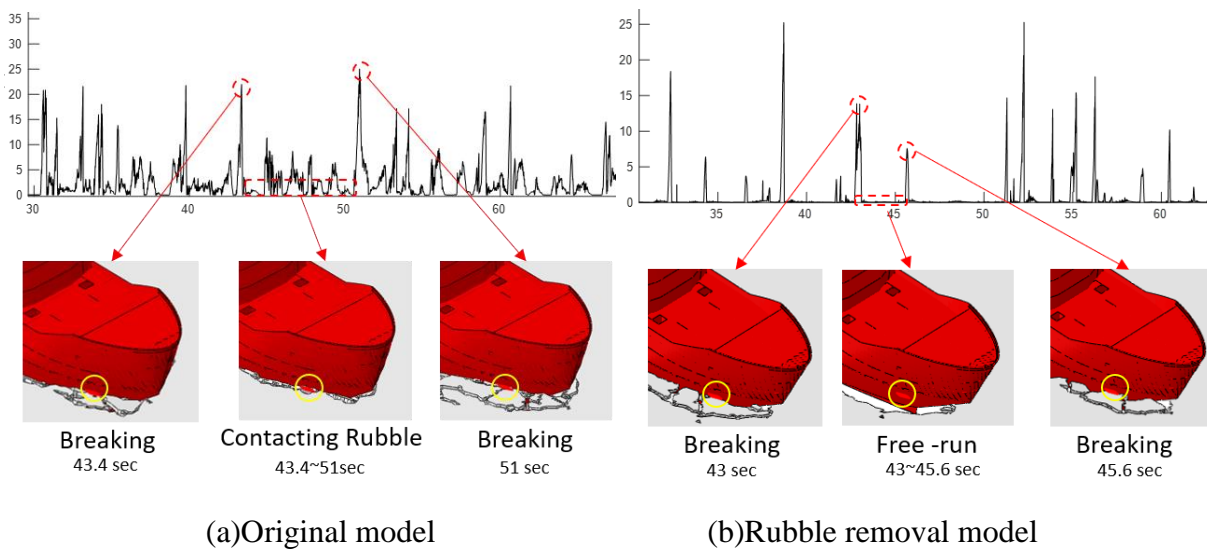


Figure 8. Comparison of local ice load original model and rubble removal model

Contribution of breaking and submersion resistance

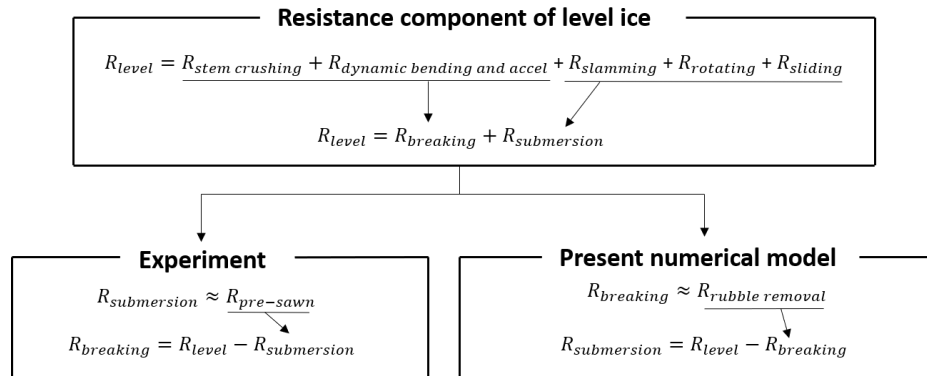


Figure 9. Difference in estimating resistance components process from numerical simulation and experiment

Figure 9 shows that there is a difference of process between simulation and experiment to obtain $R_{breaking}$ and $R_{submersion}$ of Eq(13). A pre-sawn test is a test that idealized cracks of the circumference and radial to estimate the remaining resistance except breaking component. And the breaking resistance component was calculated by subtracting $R_{pre-sawn}$ from the resistance of the level ice resistance test. On the other hand, present study directly estimated the breaking component using the rubble removal model and then calculated submersion component by subtracting resistance of rubble removal model ($R_{rubble\ removal}$) from resistance of the original model. Figure 10 is a bar graph that compares the contributions of ice resistance obtained from the result of experiment and the simulation. The blue color is the simulation result, the red color is the model test. there are differences in the proportion of the components. The resistance contribution obtained through the simulation is 20% to 30% for the breaking component, 70% to 80% for the remaining component, and 30% to 40% for the pre-sawn component, and 60% to 70% for the remaining component. Remaining component is a resistance component estimated by subtracting the total resistance (R_{level}) from the resistance obtained by pre-sawn test and rubble removal model. The variation of resistance components with respect to speed in present numerical simulation is similar with Figure 2

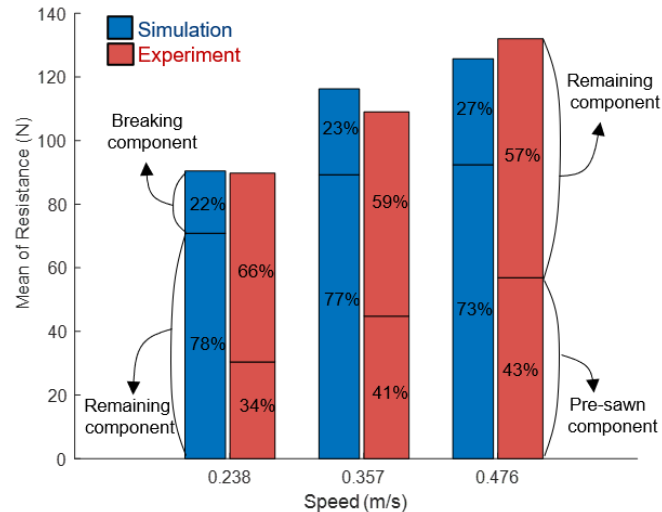


Figure 20. Contribution of breaking and submersion resistance

SUMMARY AND FURTHER STUDIES

- The ice load acting on the Araon model ship was calculated by applying the proposed simulation technique and compared it with the results of the model test. It was confirmed that this simulation adequately shows the occurrence of radial and circumferential cracks during continuous breaking.
- The resistance components were divided into breaking components and submersion components using the rubble removal model. The results of the numerical simulation were then compared with the results of the model test, which showed that the ice resistance components obtained from the present numerical simulation follow the trend of previous studies.
- The probability distribution of ice flake size was obtained by measuring the radial size of the ice flakes. As the speed increases, ice flake size decreased due to the dynamic effect, which is in line with experimental data.
- To improve the accuracy of numerical simulation, more advanced model that can take into account different tensile and compressive strength is required. Also, rate dependent material model, and more realistic hydrodynamic model needs to be taken into account.

ACKNOWLEDGEMENTS

This work was supported by the Industrial Technology Innovation Program (20008632, Development of Integrated Health Management System for Polar Operation Ships and Offshore Structures Based on Satellite Data) funded By the Ministry of Trade, Industry & Energy(MOTIE, Korea)

REFERENCES

Jeon, S.K, Kim, Y., 2021. Numerical simulation of level ice–structure interaction using damage-based erosion model, *Ocean Engineering*, 2021, 220: 108485.

Jeong, S.Y.,2016. *Ice resistance prediction method based on icebreaking pattern and ice-hull contact condition*. Ph.D. Pusan: Korea Maritime and Ocean University.

Kim, J.H., Kim, Y., 2019(a). Numerical simulation on the ice-induced fatigue damage of ship structural members in broken ice fields. *Marine Structures*, 66, pp.83-105.

Lubbad, R., Løset, S., 2011. A numerical model for real-time simulation of ship-ice interaction. *Cold Regions Science and Technology*, 62(5), pp.111-127.

Lu, W., 2014. *Floe ice-sloping structure interactions*. Ph.D. trondheim: Norwegian University of Science and Technology.

Ren, D., Sin, W. J., Kim, D. H., Park, J. C., Jeong, S. Y. ,2020. Particle-based Numerical Simulation of Continuous Ice Breaking Process around Wedge-type Model Ship. *Journal of the Society of Naval Architects of Korea*, 57(1), pp.23-34.

Zhang, N., Zheng, X., Qingwei M, 2017.Updated Smoothed Particle hydrodynamics for Simulating Bending and Compression Failure Progress of Ice, *Water*, 9(11), 882